J. Biochem. 2010;148(2):209–215 doi:10.1093/jb/mvq058

JB THE JOURNAL OF BIOCHEMISTRY

NMR and biophysical elucidation of structural effects on extra N-terminal methionine residue of recombinant amphibian RNases from *Rana catesbeiana*

Received April 8, 2010; accepted May 19, 2010; published online June 3, 2010

Chun-Hua Hsu[1,2,*], Yun-Ru Pan[2,3], You-Di Liao[2], Shih-Hsiung Wu[4] and Chinpan Chen[2,†]

[1]Department of Agricultural Chemistry, National Taiwan University, Taipei 106, Taiwan; [2]Institute of Biomedical Sciences; [3]Institute of Bioinformatics and Structural Biology, National Tsing-Hua University, Hsinchu 300; and [4]Institute of Biological Chemistry, Academia Sinica, Taipei 115, Taiwan

*Chun-Hua Hsu, Department of Agricultural Chemistry, National Taiwan University, Taipei 116, Taiwan. Tel: +886 2 33664468, Fax: +886 2 33664468, E-mail: andyhsu@ntu.edu.tw

†Chinpan Chen, Institute of Biomedical Sciences, Academia Sinica, Taipei 115, Taiwan. Tel: +886 2 26523035, Fax: +886 2 27887641, E-mail: bmchinp@ibms.sinica.edu.tw

The stability, structures and steric hindrances of recombinant RNases 2 and 4 expressed in bacteria were studied by circular dichroism (CD) and NMR techniques, and the results were compared with those of their authentic RNases extracted from oocytes of *Rana catesbeiana*. Although the overall structures of the recombinant and authentic proteins are almost identical, the extra N-terminal Met residue of the recombinant protein remarkably affects catalytic activity and stability. NMR chemical shift comparison of recombinant RNases and the authentic proteins indicated that the structural differences are mainly confined to the N-terminal helical and S2 anti-parallel β-sheet regions. Significant shift changes for the residues located on the S2 region indicate that the major influences on the structure around the N terminus is due to the loss of the hydrogen bond between Pyr^{1} and $Val^{95(96)}$ in recombinant RNases 2 and 4. We concluded the apparent steric hindrances of the extra Met to the binding pocket. As well, the affected conformational changes of active residues are attributed to the reduced activities of recombinant RNases. The structural integrity exerted by the N-terminal Pyr^{1} residue may be crucial for amphibian RNases and the greatest structural differences occur on the network of the Pyr^{1} residue and S2 β-sheet region.

Keywords: N-terminal extra methionine/NMR/protein stability/pyroglutamate/ribonuclease.

Abbreviations: CD, circular dichroism; DQF-COSY, double quantum-filtered scalar-correlated spectroscopy; NMR, nuclear magnetic resonance; NOE, nuclear Overhauser enhancement; NOESY, nuclear Overhauser enhancement spectroscopy; nRNase, native ribonuclease; Pyr, pyroglutamate; rRNase, recombinant ribonuclease; TOCSY, total correlation spectroscopy.

Ribonucleases (RNases) are widely found within living organisms and are best known for their important role in the metabolism of RNA (*1*). However, a growing number of members of the RNase A superfamily have shown unusual biological functions in addition to their intrinsic ribonucleolytic activities (*2–4*). For example, in human ribonucleases, eosinophil cationic protein (ECP, hRNase 3) and eosinophil-derived neurotoxin (EDN, hRNase 2) (*5*) show anti-parasitic and neurotoxicity activity, respectively. Angiogenin (hRNase 5) induces blood vessel formation (*6*), and amphibian RNases have anti-tumour activities (*7*, *8*). hRNases 3, 5 and 7 have been found to possess anti-microbial activities (*9*). Ribonucleolytic activity is essential to the biological functions of these proteins.

Amphibian RNases from the *Rana* species, possessing pyroglutamate (Pyr) at the N terminus, are known to have high thermostability and are not neutralized by the ribonuclease inhibitor from human placenta (*8*, *10–13*). Among them, onconase from *Rana pipiens* is the best known and is currently being evaluated in combination with tamoxifen (*14*) and doxorubicin (*15*) as tumour therapy in human phase III clinical trials. Because amphibian RNases present therapeutic opportunities for tumour cell and viral diseases (*16*), large-scale protein production is the next significant step for potential as therapeutic protein drugs. The *Escherichia coli* system is effective for expressing high-yield proteins (*8*, *17*), but sequestered in inclusion bodies. After the refolding process, the protein can be obtained; however, the recombinant protein is often produced with an extra methionine (Met^{-1}) at the N terminus.

In this study, to thoroughly examine the effect of an additional Met^{-1} and Glu^{1} instead of a Pyr residue on the conformational stability and the biological property of frog RNases, we compared two small recombinant RNases (rRNases 2 and 4) from *Rana catesbeiana* with their native proteins using biophysical approaches. The multiple sequence alignment of the four frog RNases is shown in Fig. 1; the sequence identity ranges from 53% to 66% with onconase used as a reference. The biological assay revealed that the frog rRNases have lower activities than do native RNases (nRNase). Circular dichroism (CD) studies showed that the recombinant proteins with an extra residue at the N terminus were significantly destabilized. Comparison of NMR spectra of recombinant and native proteins show the structural effects of the extra Met^{-1}. We discuss the results of structural analyses and biological properties, as well as the effect of an additional N-terminal Met^{-1}.

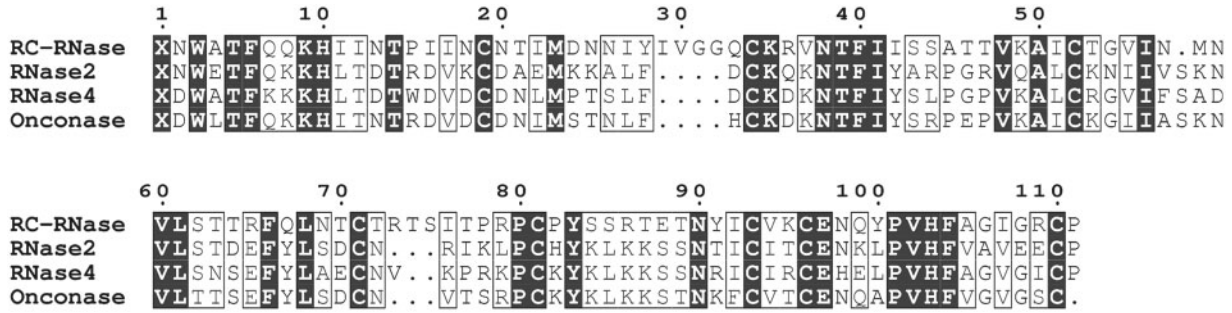

Fig. 1 Sequence alignments of *R. catesbeiana* RNase (RC-RNase), RNase 2, RNase 4 and onconase. The sequence number on the top is based on the sequence of RC-RNase. The pyroglutamate (Pyr) residue is indicated by a single letter 'X'. Residues that are identical are shown in white type with a black background and those that are highly conserved are shown within boxes.

Materials and Methods

Preparation of native and rRNases

nRNases 2 and 4 were purified from *R.catesbeiana* (bullfrog) oocytes as described previously (*8*). The bullfrogs were obtained from a local frog farm. Purification of oocyte RNases was carried out at 4°C. Ovaries (60-100 g per frog) from mature female bullfrogs underwent ultracentrifugation for 45 min at 100,000*g* with use of a Beckman SW41 rotor. The yolk granules containing most of the RNases in the pellet were extracted by NaCl (*13*). The clear supernatant was applied onto a phosphocellulose column and eluted with a 0.09- to 0.7-M KCl gradient in buffer A (19 mM HEPES, pH 7.9, 0.1 mM EDTA).

The rRNases with an extra Met^{-1} at the N terminus were produced in *E. coli* BL21 (DE3) from the rRNases 2 and 4 genes, cloned in pET-22b (Novagen) and induced by isopropyl-β-thiogalactopyranoside. The inclusion bodies were collected after the cells were lyzed by microfluidizer and resolved in 6 M GdnHCl at room temperature for 1 h. The refolding solution was concentrated and dialysed against sodium acetate (pH 5.0) and then underwent carboxymethyl cellulose (CM52, Whatman) and FPLC mono S (Pharmacia) column chromatography. SDS–PAGE and ES/MS spectrometry were used to confirm the derived proteins.

Assay of ribonuclease activity

Ribonuclease activities were analysed by zymography on the RNA-casting PAGE (*18*). Briefly, after electrophoresis, the gel was washed twice with 25% isopropyl alcohol in 10 mM Tris–HCl, pH 7.5, to remove SDS for protein renaturation. The activity was visible after incubating the gel at room temperature for 30 min in 10 mM Tris–HCl, pH 7.5, and staining by 0.2% toluidine blue O for 10 min. The RNase activities of each native and recombinant protein were determined by the release of acid-soluble nucleotides from Bakers yeast total RNA after RNase digestion in 50 mM sodium acetate (pH 6.0). The specific activity of the enzyme was defined as the increase in absorbance at 260 nm by 1 μg ribonuclease at 37°C for 15 min. The specific cleavage sites on RNA were determined by incubating RNases with 5′-AAGGUUAUCCGCACUGAA-3′, then denaturing gel electrophoresis and autoradiography.

Assay of conformational stability

CD experiments involved use of an Aviv 202 SF CD spectrometer (Lakewood, NJ, USA) calibrated with (+)-10-camphorsulfonic acid at 25°C. In general, a 2-mm path-length cuvette with 20 μM nRNases or rRNases in 20 mM phosphate buffer was used for CD experiments, and all the protein solutions were made up to 1 ml. The steady-state CD spectra were recorded from 260 to 180 nm at different temperatures and pH values. After background subtraction and smoothing, all the CD data were converted from CD signal (millidegree) to mean residue ellipticity (deg cm^2 $dmol^{-1}$). The secondary structure content was estimated from the CD spectra by use of CONTIN, SELCON and CDSSTR (*19*) in the CDpro program.

Equilibrium thermal-denaturing experiments were performed by measuring the change in molar ellipticity at 228 nm. Data were collected as a function of temperature, with a scan rate of 2 min deg^{-1} over a range of 20–95°C in 20 mM phosphate buffer, pH 7.0. The variation was monitored at 228 nm after 3-min equilibration at each point with a temperature controller. The reversibility was checked by monitoring the changes of ellipticity on cooling the heated sample. The enthalpy and heat capacity changes of unfolding were determined by assuming the two-state transition. The thermal unfolding transition curve was fitted to the following equations:

$$[\theta]_{obs} = \frac{[\theta]_N + [\theta]_U \exp(-\Delta G(T)/RT)}{1 + \exp(-\Delta G(T)/RT)} \quad (1)$$

$$\Delta G(T) = \Delta H(T_m)\left(\frac{1-T}{T_m}\right) + \Delta C_p\left\{T - T_m - T\ln\left(\frac{T}{T_m}\right)\right\}, \quad (2)$$

where $[\theta]_{obs}$, $[\theta]_N$ and $[\theta]_U$ are the ellipticity at a given temperature of the native conformation and the unfolded conformation, respectively. $\Delta G(T)$ is the unfolding free energy change at an absolute temperature T. T_m is the melting temperature, $\Delta H(T_m)$ is the unfolding enthalpy change at T_m and ΔC_p is the heat capacity change of unfolding.

NMR spectroscopy

All NMR experiments were recorded at 310 K on a Bruker AVANCE 600 spectrometer equipped with a triple (^1H, ^{15}N and ^{13}C) resonance probe including shielded z-gradients. 2D ^1H NMR spectra (*20*) from scalar-correlated spectroscopy (COSY), total correlation spectroscopy (TOCSY), nuclear Overhauser enhancement spectroscopy (NOESY) and deuterium–hydrogen exchange experiments were collected at different temperatures (303 K, 310 K and 320 K) for nRNases 2 and 4. All heteronuclear NMR experiments for rRNases were performed as described (*21*). Linear prediction was used in the ^{13}C and ^{15}N dimensions to improve the digital resolution. 2,2-dimethyl-2-silapentane-5-sulphonate was used as an external chemical shift standard at 0.00 ppm. The ^{15}N and ^{13}C chemical shifts were indirectly referenced by use of the consensus ratios of the zero-point frequencies at 310 K (*22*, *23*). All spectra were processed by use of XWIN-NMR and analysed by AURELIA on an SGI O_2 workstation.

Results

Conformational stability and secondary structure based on CD data

The catalytic activities of nRNases and rRNases were assayed by zymography on RNA-casting SDS–PAGE (Fig. 2A). The catalytic activities were reduced by the additional Met^{-1} in the bacterially expressed frog RNases. However, the base specificities of rRNases were not altered (Fig. 2B). Interestingly, CD spectra of the native and recombinant proteins acquired under identical conditions are similar, which reveals that they possess a similar secondary structure (Fig. 3). Therefore, the extra Met does not significantly affect the overall structure and should only make a

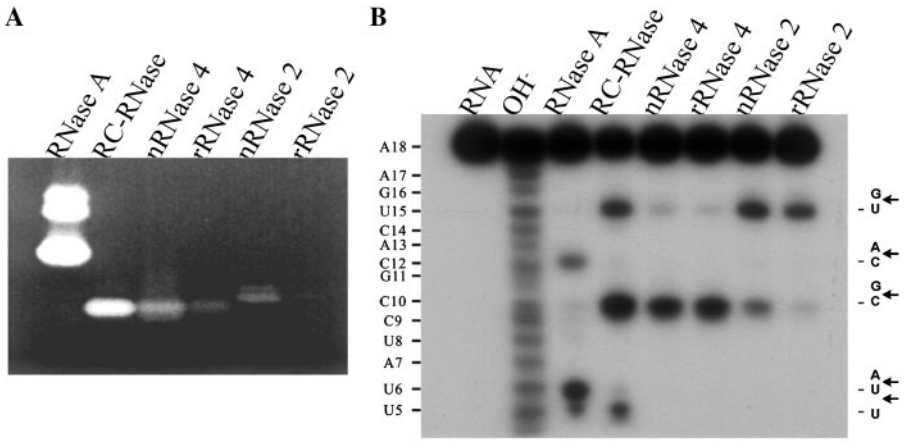

Fig. 2 Comparison of RNase activities and base specificities for nRNase and rRNase. (A) Zymography analysis. RNase A, RC-RNase, nRNases 2 and 4 and rRNases 2 and 4 were subjected to 13.3% RNA-casting SDS–PAGE and assayed for their activities. (B) Base specificity. An 18-mer 5′-end-labelled RNA was partially digested with RNase A, RC-RNase, nRNases 2 and 4 and rRNases 2 and 4 a rRNase were subjected to 8 M urea–15% PAGE separation and autoradiography. OH^- indicates that the RNA substrate was treated with 0.05 M sodium bicarbonate–carbonate at pH 9.2 and at 90°C for 4 min. The RNA sequence and cleavage sites are shown in the left and right margins, respectively.

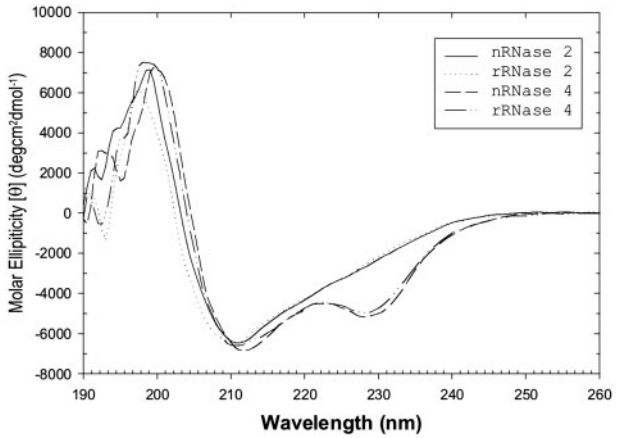

Fig. 3 Comparison of steady-state CD spectra of 20 μM nRNases 2 and 4 and rRNases 2 and 4 dissolved in 20 mM phosphate buffer at pH 7.0. The CD data for native and recombinant RNases under the identical conditions are comparable, which indicates that their secondary structures and tertiary folds are similar.

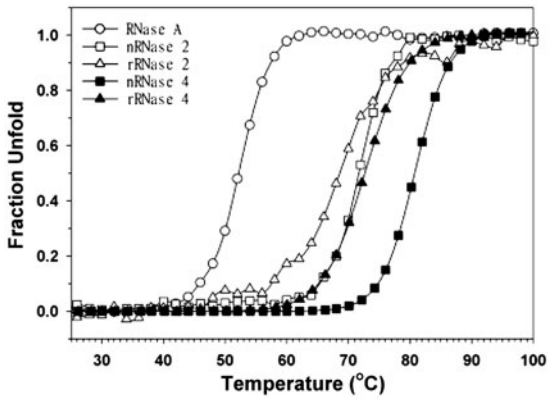

Fig. 4 Equilibrium CD titration experiments as a function of temperature for frog nRNases and rRNases compared with RNase A. The thermostability of these proteins was measured at pH 7.0. The T_m value of nRNase 2 is near 71.5°C. rRNase 2 has a reduced T_m values of about 68.5°C. In addition, the T_m value for nRNase 4 is near 80°C and rRNase 4 has a reduced T_m value of about 72°C. For comparison, the T_m (52°C) of RNase A is much smaller than those for nRNases and rRNases.

minor structural difference, to cause the decrease in catalytic activity for rRNases. Both nRNase 4 and rRNase 4 have two negative ellipticities at 212 nm and 228 nm; however, the CD spectra for both nRNase 2 and rRNase 2 show only a single minimum, at 211 nm. The distinct negative mean residue molar ellipticity for nRNase 4 and rRNase 4 at 228 nm arises from the interaction of the tryptophan side chain (Trp^{15}) with the backbone of its nearby residues.

CD melting studies were then performed to investigate the protein stability. As shown in Fig. 4, T_m values of 71.5°C and 68.5°C were obtained for nRNase 2 and rRNase 2, respectively, on the basis of equilibrium titration experiments at different temperatures from 10°C to 100°C at pH 7.0. Different T_m values of 72°C and 80°C were also obtained for rRNase 4 and nRNase 4, respectively, under the same experimental condition. T_m, $\Delta H(T_m)$ and ΔC_p were obtained by curve fitting (Table I). Comparison of the T_m value between the recombinant and nRNases indicated that the additional N-terminal Met^{-1} influences the stability of the protein or interrupts the intramolecular interaction. On the basis of T_m and $\Delta H(T_m)$, ΔG at T_m for native and recombinant RNases 2 and 4 was calculated by Equation 2, and is in Table I. rRNases 2 and 4 are less stable by 1.8 and 7.3 kJ mol^{-1}, respectively, than their native proteins. Solution structure comparison of rRNases 2 and 4 (*11*) revealed the slight difference in the N-terminal helix (α1) orientation. The strikingly apparent ΔG difference between rRNase 2 and rRNase 4 may occur because of the different perturbing level of the additional Met^{-1} and uncyclized Gln^1. Furthermore, the N-terminal extra Met^{-1} should encumber the folding progress of these two RNases with different N-terminal helix orientation at the different disturbance levels.

Table I. Thermodynamic parameters for the unfolding of native and recombinant RNases.

Protein name	Native protein	Recombinant protein
RNase 2		
T_m (°C)	71.5	68.5
$\Delta H(T_m)$ (kJ mol^{-1})	362.4 ± 3.6	199.8 ± 0.9
ΔC_p (kJ mol^{-1} K^{-1})	7.1 ± 0.7	2.6 ± 0.2
$\Delta G(T_m)$ (kJ mol^{-1})	0	−1.8
RNase 4		
T_m (°C)	80	72
$\Delta H(T_m)$ (kJ mol^{-1})	393.8 ± 1.2	299.2 ± 0.8
ΔC_p (kJ mol^{-1} K^{-1})	4.4 ± 0.2	2.6 ± 0.2
$\Delta G(353)$ (kJ mol^{-1})	0	−7.3

Comparison of NMR data for native and recombinant ($M^{-1}(Q^1)$) RNases

NMR techniques were used to further examine the structural similarities between nRNases and rRNases. Figure 5A and B show the superimposition of the fingerprint region of two TOCSY spectra between native and recombinant proteins. Most of the residues displayed identical chemical shifts, which indicates that their tertiary structures are similar. Further NMR resonance assignments were performed to define the conformational differences. Assignments for the backbone resonances of rRNases 2 and 4 were completed by the 3D NMR experiment and deposited into BioMagResBank under Accession numbers BMRB-4825 (*24*) and BMRB-4893 (*25*), respectively. By comparing the chemical shifts of the H^N-Hα

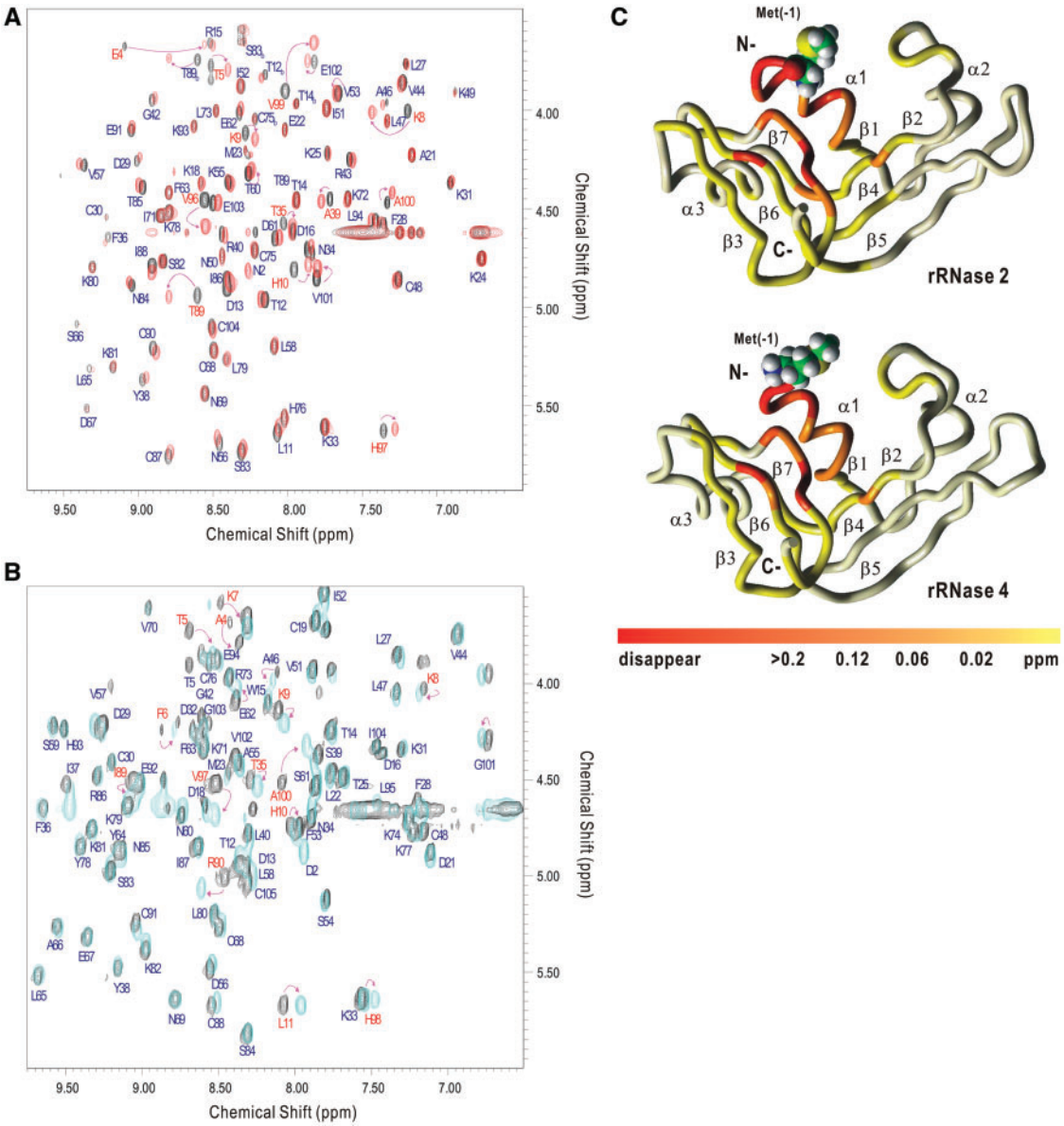

Fig. 5 NMR parameters between native and recombinant RNases. Comparison of 2D HSQC spectra for nRNases 2 and 4 and rRNases 2 and 4 are shown in (A) and (B), respectively. Because of the effect of the extra Met^{-1} residues at the N terminus in the recombinant protein, a few small regions of chemical shifts are different. (C) Representative ribbon structures showing chemical shift perturbation of rRNases 2 and 4. The chemical shift differences between the native and recombinant proteins are coloured from red to yellow.

cross-peaks of rRNases and nRNases, we obtained unambiguous assignments for well-resolved cross-peaks. To avoid erroneous assignments for the crowded part of the fingerprint region (H^N-Hα), we used the standard sequential assignment procedure (*26*). The large shifted residues are annotated in Fig. 5A and B.

Chemical shift differences between recombinant and nRNases

NMR chemical shifts are sensitive probes for the environments where each spin is located in the 3D structure of protein molecules. If the solution conformations of the two forms of RNases differ, some spins should show chemical shift differences. In total, 54 and 45 amino acids showed shifted resonances between nRNase 2 and rRNase 2 and between nRNase 4 and rRNase 4, respectively (Fig. 5A and B). The notable shifted peaks were observed on Glu^4, Thr^5, Lys^8, Thr^{89} and Val^{96} in rRNase 2 and Ala^4, Thr^5, Arg^{90} and Val^{97} in rRNase 4, all of which are confined to the N-terminal helical region and S2 anti-parallel β-sheets. In addition, the neighbouring residues of Val^{96} and Val^{97} in rRNases 2 and 4, respectively, have minor chemical shift differences. Considering that the only structural difference between the two forms of RNases is the presence of the additional Met residue at the N terminus of rRNases, the chemical shift change observed for the Val on the β7 strand is intriguing. To confirm that the chemical shift difference is not due to environmental differences, such as different buffers, NMR experiments were performed of native and recombinant N^{15}-labelled proteins mixed in the same buffer. 2D-TOCSY with decoupling and 2D-version NOESY-N^{15}-HSQC were measured and overlaid for comparison. The same significant change was observed in the mixed sample.

Discussion

In summary, our investigation suggests that the structural integrity exerted by the N-terminal Pyr^1 residue is crucial for frog RNases and that the most structural differences occur on the network of the Pyr^1 residue and the S2 sheet region. We provide structural insight into the importance of the Pyr residue and provide further understanding for developing therapeutic protein drugs from the cytotoxic frog RNases.

Of proteins with a signal peptide, 12.3% are initiated with Gln at the N terminus after the signal peptide is removed. The resulting N-terminal Gln is converted to Pyr by deamination, which is usually essential for the biological functions of many proteins and hormones (*27*, *28*). RNases with Pyr at the N terminus, with cytotoxicity towards tumour cells, are predominantly found in the oocytes of frog. With respect to the N-terminal Pyr in ribonucleases, the N-terminal Pyr of human angiogenin (*29*) or human RNase 4 (*30*) is structurally flexible and not involved in catalytic activity. Also, Pyr is observed at the N terminus of most mouse RNases, but its function is still not clear (*31*).

Many proteins expressed in *E. coli* have the N-terminal Met residue, although whether the Met residue is present or not depends on the penultimate residue in the recombinant protein (*32*). However, the effects of such an extra residue have been usually ignored. After bacterial expression, refolding and purification, we obtained a large amount of frog rRNase with an extra Met^{-1} at the N terminus exhibiting remarkably reduced catalytic activity. Thus, we investigated the effect of the N-terminal Met on the structure, stability and other properties by biochemical and biophysical methods. The structural effect of protein stability and folding by an extra Met for recombinant α-lactalbumin (*33*) and human lysozyme (*34*) have been reported; the crystal structure was determined to compare the difference between native and recombinant proteins. The crystal structure of recombinant human lysozyme revealed that the expanded N-terminal residue caused the destruction of hydrogen bond networks with an ordered water molecule. Studies on α-lactalbumin suggest that the extra Met destabilizes the native state through a conformational entropy effect. However, the N-terminal Met may affect the molecular packing in the crystal because the space group is altered in the recombinant protein crystal (*33*). Here, we investigated the structural aspects that explain differences in thermostability and structural differences between the recombinant and native proteins on the basis of our CD and NMR data in the ideal condition.

The similarities of CD spectra between recombinant and nRNases indicate that the extra Met^{-1} should not influence the tertiary fold for the recombinant protein. However, equilibrium CD titration experiments showed the T_m values reduced in the recombinant protein with an additional Met^{-1} and uncyclized Gln^1. We analysed the NMR spectra of both recombinant and native proteins to check for differences in residues. The overall structures of these two forms are essentially identical, which is consistent with the identical CD spectra of the proteins, and structural differences between the proteins are localized in the N terminus and the β6-7 strand regions (Fig. 5C). Because the structural differences in the β6-7 strand regions, which contain the active-site residue of His, are likely caused by losing the hydrogen bonding formed with Pyr^1, we concentrated our attention on the structural differences in the β6-7 regions and investigated the interactions present in native proteins but missing in the recombinant proteins.

Our previous study showed three hydrogen bonds bind to Lys^9, Val^{102} and Lys^{95} exerted by Pyr^1 and other hydrogen bonds bound to Tyr^{28}, Asn^{38} and substrates by these related residues in *R. catesbeiana* RNases (*11*, *35*). The hydrogen bond network contributed by these residues at different α-helices, β-strands and loops is able to strengthen the structural integrity of RNases; example of residues are Pyr^1 (α1), Lys^9 (α1), Val^{102} (β6), Tyr^{28} (1oop2), Asn^{38} (β1) and Lys^{95} (β5) in RC-RNase. According to the modelled structures of nRNases 2 and 4 generated with crystal structure of RC-RNase used as a template, Pyr^1 of the nRNases is hydrogen bonded, with the side chain of Lys^9 and the backbone of Val^{96} and Val^{97} in RNases 2 and 4, respectively. The corresponding residues of RNases 2 and 4 to those in RC-RNase are in

Table II. Chemical-shift changes on Pyr^1 and the residues that form hygrogen bonds with Pyr^1, as well as the active site residues in RC-RNases 2 and 4.

RC-RNase	RNase 2	Δppm	RNase 4	Δppm
Pyr^1	Pyr^1	ND	Pyr^1	ND
Lys^9	Lys^9	0.06 (H^N)	Lys^9	0.04 (H^N)
		−0.03 (Hα)		−0.06 (Hα)
Val^{102}	Val^{96}	0.00 (H^N)	Val^{97}	0.00 (H^N)
		−0.15 (Hα)		−0.15 (Hα)
Tyr^{28}	Phe^{28}	−0.02 (H^N)	Phe^{28}	0.03 (H^N)
		0.01 (Hα)		−0.03 (Hα)
Asn^{38}	Asn^{34}	0.00 (H^N)	Asn^{34}	0.00 (H^N)
		0.04 (Hα)		0.02 (Hα)
Lys^{95}	Thr^{89}	−0.20 (H^N)	Arg^{90}	−0.15 (H^N)
		0.00 (Hα)		−0.05 (Hα)
Ala^{105}	Val^{99}	0.20 (H^N)	Ala^{100}	0.13 (H^N)
		0.25 (Hα)		0.21 (Hα)
Active sites				
His^{10}	His^{10}	0.10 (H^N)	His^{10}	0.05 (H^N)
		0.02 (Hα)		−0.02 (Hα)
Thr39	Thr^{35}	0.10 (H^N)	Thr^{35}	0.06 (H^N)
		0.02 (Hα)		−0.02 (Hα)
His103	His^{97}	0.09 (H^N)	His^{98}	0.07 (H^N)
		0.00 (Hα)		0.00 (Hα)

Table I. The chemical shift differences of these residues between recombinant and native proteins are also presented. The resonances of Val^{96} and Thr^{89} in rRNase 2 and Val^{97} and Arg^{90} in rRNase 4 are apparently shifted from their native ones. The changes should be caused by the loss of the hydrogen bond between Nα of Pyr^1 and the backbone carbonyl group of Val^{96} in rRNase 2 and Val^{97} in rRNase 4, which further form hydrogen bonds to Thr^{89} and Arg^{90} in rRNases 2 and 4, respectively. In addition, the Val^{99} of rRNase 2 and Ala^{100} of rRNase 4, being equivalent to Ala^{105} of RC-RNase, show the shifted resonances.

The hydrogen bond between Pyr^1 to Lys^9 does not significantly influence the shift perturbation between native and recombinant proteins (Table II). Lys^9 is also bound to Tyr^{28} and the side chain amide of Asn^{38} in RC-RNase, which are observed at the equivalent residues of Phe^{28} and Asn^{34} in RNases 2 and 4. The active sites, His^{10}, Thr^{39} and His^{102} of RC-RNase, as well as the equivalent residues of RC-RNases 2 and 4 are also shown in Table I. Thus, the activity loss of recombinant RNase is due to the steric hindrance to the binding pocket and conformational changes of the active residues.

In conclusion, our study shows that the presence of the additional N-terminal Met^{-1} in recombinant RC-RNases expressed in *E. coli* decreasing the stability of the recombinant proteins is mainly due to the loss of important hydrogen bonds. Furthermore, the hydrogen bond between Pyr^1 and the S2 anti-parallel sheet region is critical to protein stability. The hydrogen bond network contributed by these residues at the S2 β-sheet is important to strengthen the structural integrity of RNases. The structural properties and conformational stabilities of recombinant amphibian RNases can depend on the peculiarities of the extra Met^{-1} residue. The reduced stabilities of protein may be related to the decreased activities of rRNase. In addition, the modification of the N-terminal Pyr of RNases perturbs the B1 and B2 sites slightly, but does not significantly affect its base specificity. However, the apparent steric hindrances of the extra Met^{-1} to the binding pocket and the affected conformations of active residues monitored by chemical shift differences correspond to the reduced activities of rRNases.

Acknowledgements

C.-H.H. is a visiting scholar in the Institute of Biomedical Sciences, Academia Sinica. The NMR spectra were obtained at the High-Field Biomacromolecular NMR Core Facility for Proteomic Research, National Research Program for Genomic Medicine, Taiwan.

Funding

This work was supported in part by the research grant from National Science Council (NSC 97-2113-M-002-005-MY2 and NSC 96-2113-M-002-028-MY2) and by Academia Sinica, Taiwan.

Conflict of interest

None declared.

References

1. D'Alessio, G. (1993) New and cryptic biological messages from RNases. *Trends Cell Biol.* **3**, 106–109
2. Pizzo, E. and D'Alessio, G. (2007) The success of the RNase scaffold in the advance of biosciences and in evolution. *Gene* **406**, 8–12
3. Dyer, K.D. and Rosenberg, H.F. (2006) The RNase a superfamily: generation of diversity and innate host defense. *Mol. Divers.* **10**, 585–597
4. Loverix, S. and Steyaert, J. (2003) Ribonucleases: from prototypes to therapeutic targets? *Curr. Med. Chem.* **10**, 779–785
5. Gleich, G.J., Loegering, D.A., Bell, M.P., Checkel, J.L., Ackerman, S.J., and McKean, D.J. (1986) Biochemical and functional similarities between human eosinophil-derived neurotoxin and eosinophil cationic protein: homology with ribonuclease. *Proc. Natl Acad. Sci. USA* **83**, 3146–3150
6. Shapiro, R., Riordan, J.F., and Vallee, B.L. (1986) Characteristic ribonucleolytic activity of human angiogenin. *Biochemistry* **25**, 3527–3532
7. Wu, Y., Mikulski, S.M., Ardelt, W., Rybak, S.M., and Youle, R.J. (1993) A cytotoxic ribonuclease. Study of the mechanism of onconase cytotoxicity. *J. Biol. Chem.* **268**, 10686–10693
8. Liao, Y.D., Huang, H.C., Leu, Y.J., Wei, C.W., Tang, P.C., and Wang, S.C. (2000) Purification and cloning of cytotoxic ribonucleases from *Rana catesbeiana* (bullfrog). *Nucleic Acids Res.* **28**, 4097–4104
9. Huang, Y.C., Lin, Y.M., Chang, T.W., Wu, S.J., Lee, Y.S., Chang, M.D., Chen, C., Wu, S.H., and Liao, Y.D. (2007) The flexible and clustered lysine residues of human ribonuclease 7 are critical for membrane permeability and antimicrobial activity. *J. Biol. Chem.* **282**, 4626–4633
10. Rutkoski, T.J. and Raines, R.T. (2008) Evasion of ribonuclease inhibitor as a determinant of ribonuclease cytotoxicity. *Curr. Pharm. Biotechnol.* **9**, 185–189
11. Hsu, C.H., Liao, Y.D., Pan, Y.R., Chen, L.W., Wu, S.H., Leu, Y.J., and Chen, C. (2003) Solution structure of the cytotoxic RNase 4 from oocytes of bullfrog Rana catesbeiana 1H, 13C and 15N resonance assignments and

secondary structure of the cytotoxic protein RNase 4 from bullfrog *Rana catesbeiana* oocytes 1H, 15N and 13C resonance assignments and secondary structure determination of the RC-RNase 2 from oocytes of bullfrog *Rana catesbeiana*. *J. Mol. Biol.* **326**, 1189–1201
12. Irie, M., Nitta, K., and Nonaka, T. (1998) Biochemistry of frog ribonucleases. *Cell. Mol. Life. Sci.* **54**, 775–784
13. Liao, Y.D., Huang, H.C., Chan, H.J., and Kuo, S.J. (1996) Large-scale preparation of a ribonuclease from *Rana catesbeiana* (bullfrog) oocytes and characterization of its specific cytotoxic activity against tumor cells. *Protein Expr. Purif.* **7**, 194–202
14. Lee, I., Lee, Y.H., Mikulski, S.M., and Shogen, K. (2003) Effect of ONCONASE +/− tamoxifen on ASPC-1 human pancreatic tumors in nude mice. *Adv. Exp. Med. Biol.* **530**, 187–196
15. Mikulski, S.M., Viera, A., Deptala, A., and Darzynkiewicz, Z. (1998) Enhanced in vitro cytotoxicity and cytostasis of the combination of onconase with a proteasome inhibitor. *Int. J. Oncol.* **13**, 633–644
16. Saxena, S.K., Gravell, M., Wu, Y.N., Mikulski, S.M., Shogen, K., Ardelt, W., and Youle, R.J. (1996) Inhibition of HIV-1 production and selective degradation of viral RNA by an amphibian ribonuclease. *J. Biol. Chem.* **271**, 20783–20788
17. Notomista, E., Cafaro, V., Fusiello, R., Bracale, A., D'Alessio, G., and Di Donato, A. (1999) Effective expression and purification of recombinant onconase, an antitumor protein. *FEBS Lett.* **463**, 211–215
18. Liao, Y.D. and Wang, J.J. (1994) Yolk granules are the major compartment for bullfrog (*Rana catesbeiana*) oocyte-specific ribonuclease. *Eur. J. Biochem.* **222**, 215–220
19. Sreerama, N. and Woody, R.W. (2000) Estimation of protein secondary structure from circular dichroism spectra: comparison of CONTIN, SELCON, and CDSSTR methods with an expanded reference set. *Anal. Biochem.* **287**, 252–260
20. Bax, A. (1989) Two-dimensional NMR and protein structure. *Annu. Rev. Biochem.* **58**, 223–256
21. Kay, L.E. (1995) Pulsed field gradient multi-dimensional NMR methods for the study of protein structure and dynamics in solution. *Prog. Biophys. Mol. Biol.* **63**, 277–299
22. Wishart, D.S. and Sykes, B.D. (1994) Chemical shifts as a tool for structure determination. *Methods Enzymol.* **239**, 363–392
23. Wishart, D.S., Bigam, C.G., Yao, J., Abildgaard, F., Dyson, H.J., Oldfield, E., Markley, J.L., and Sykes, B.D. (1995) 1H, 13C and 15N chemical shift referencing in biomolecular NMR. *J. Biomol. NMR* **6**, 135–140
24. Hsu, C.H., Chen, L.W., Liao, Y.D., Wu, S.H., and Chen, C. (2001) 1H, 15N and 13C resonance assignments and secondary structure determination of the RC-RNase 2 from oocytes of bullfrog *Rana catesbeiana*. *J. Biomol. NMR* **19**, 87–88
25. Hsu, C.H., Liao, Y.D., Wu, S.H., and Chen, C. (2001) 1H, 13C and 15N resonance assignments and secondary structure of the cytotoxic protein RNase 4 from bullfrog *Rana catesbeiana* oocytes. *J. Biomol. NMR* **20**, 93–94
26. Wüthrich, K. (1986) *NMR of Protein and Nucleic Acids*., Wiley Interscience, New York
27. Busby, W.H. Jr, Quackenbush, G.E., Humm, J., Youngblood, W.W., and Kizer, J.S. (1987) An enzyme(s) that converts glutaminyl-peptides into pyroglutamyl-peptides. Presence in pituitary, brain, adrenal medulla, and lymphocytes. *J. Biol. Chem.* **262**, 8532–8536
28. Fischer, W.H. and Spiess, J. (1987) Identification of a mammalian glutaminyl cyclase converting glutaminyl into pyroglutamyl peptides. *Proc. Natl Acad. Sci. USA* **84**, 3628–3632
29. Shapiro, R., Harper, J.W., Fox, E.A., Jansen, H.W., Hein, F., and Uhlmann, E. (1988) Expression of Met-(-1) angiogenin in *Escherichia coli*: conversion to the authentic less than Glu-1 protein. *Anal. Biochem.* **175**, 450–461
30. Terzyan, S.S., Peracaula, R., de Llorens, R., Tsushima, Y., Yamada, H., Seno, M., Gomis-Ruth, F.X., and Coll, M. (1999) The three-dimensional structure of human RNase 4, unliganded and complexed with d(Up), reveals the basis for its uridine selectivity. *J. Mol. Biol.* **285**, 205–214
31. Batten, D., Dyer, K.D., Domachowske, J.B., and Rosenberg, H.F. (1997) Molecular cloning of four novel murine ribonuclease genes: unusual expansion within the ribonuclease A gene family. *Nucleic Acids Res.* **25**, 4235–4239
32. Miller, C.G., Strauch, K.L., Kukral, A.M., Miller, J.L., Wingfield, P.T., Mazzei, G.J., Werlen, R.C., Graber, P., and Movva, N.R. (1987) N-terminal methionine-specific peptidase in Salmonella typhimurium. *Proc. Natl Acad. Sci.USA* **84**, 2718–2722
33. Chaudhuri, T.K., Horii, K., Yoda, T., Arai, M., Nagata, S., Terada, T.P., Uchiyama, H., Ikura, T., Tsumoto, K., Kataoka, H., Matsushima, M., Kuwajima, K., and Kumagai, I. (1999) Effect of the extra n-terminal methionine residue on the stability and folding of recombinant alpha-lactalbumin expressed in *Escherichia coli*. *J. Mol. Biol.* **285**, 1179–1194
34. Takano, K., Tsuchimori, K., Yamagata, Y., and Yutani, K. (1999) Effect of foreign N-terminal residues on the conformational stability of human lysozyme. *Eur. J. Biochem.* **266**, 675–682
35. Leu, Y.J., Chern, S.S., Wang, S.C., Hsiao, Y.Y., Amiraslanov, I., Liaw, Y.C., and Liao, Y.D. (2003) Residues involved in the catalysis, base specificity, and cytotoxicity of ribonuclease from *Rana catesbeiana* based upon mutagenesis and X-ray crystallography. *J. Biol. Chem.* **278**, 7300–7309